Supporting Information

Direct Photopatterning and Erasing of Quantum Dots via Ligand Photoisomerization

Zhong Fu,†[a] Zhi Zheng,†[a] Yu Xie,†[b] Hannikezi Abudukeremu, [a] Likuan Zhou, [c] Shuangan Zang, [b] Kunfei Tian, [c] Qiuyu Liu, [c] Yuan Li [b] and Hao Zhang*[a]

a Department of Chemistry, Center for BioAnalytical Chemistry, Key Laboratory of Bioorganic Phosphorus Chemistry & Chemical Biology (Ministry of Education), Tsinghua University, Beijing 100084, China. E-mail: hzhangchem@mail.tsinghua.edu.cn

b Department of Chemistry, Key Laboratory of Organic Optoelectronics & Molecular Engineering (Ministry of Education), Tsinghua University, Beijing 100084 China.

c National Center of Technology Innovation for Display, Guangzhou, Guangdong 510525, China.

† These authors contributed equally to this work.

*To whom correspondence should be addressed.

E-mail: hzhangchem@mail.tsinghua.edu.cn.

Methods

Chemicals and materials

All chemicals and materials were used as received unless otherwise specified. Triphenylmethanethiol, potassium carbonate (anhydrous), 4-hydroxyazobenzene, trifluoroacetic acid, 1-octadecene (ODE, 90%), anhydrous ethanol (99.5%), and anhydrous chlorobenzene (99.8%) were purchased from Sigma-Aldrich. 1,10-Dibromodecane and acetonitrile were obtained from Energy Chemical. Petroleum ether, ethyl acetate, and deuterated chloroform ($CDCl_3$) were supplied by J&K Scientific. Chloroform and dichloromethane were purchased from Beijing Tongguang Fine Chemicals. Toluene (99.5%) was purchased from Fisher Scientific and further purified using an MBraun MB SPS solvent purification system. II–VI semiconductor QDs with core–shell structures emitting in red (CdZnSe/CdZnS/ZnS), green (CdZnSe/ZnSe/ZnS), and blue (CdZnSe/ZnS), as well as ZnMgO nanoparticles, were provided by TCL Inc. InP/ZnSe/ZnS QDs were purchased from Suzhou Xingshuo Nanotech Co. Ltd. PEDOT:PSS (Baytron PVP AI 4083) was purchased from Heraeus. TFB (poly[(9,9-dioctylfluorenyl-2,7-diyl)-alt-(4,4'-(N-(4-butylphenyl))]) was purchased from American Dye Source.

Synthesis of AZO ligands

The AZO ligand was synthesized according to previously reported procedures with slight modifications[1,2], as shown in Fig. S1.

Step 1. Synthesis of 1-((10-bromodecyl)thio)triphenylmethane (Br-STr)

To a 500 mL two-necked flask were added 1,10-dibromodecane (10 g, 33 mmol), Triphenylmethanethiol (1.9 g, 7 mmol), and anhydrous potassium carbonate (9.1 g, 66 mmol), followed by the addition of 250 mL of acetonitrile. The flask was purged with nitrogen for 15 minutes to remove air from the system. Subsequently, the reaction mixture was heated to reflux at 85 ºC under a nitrogen atmosphere and stirred for 18 hours. After the reaction was complete, the mixture was cooled to room temperature, and the solid was removed by filtration. The solvent was removed by using a rotary evaporator. The crude product was purified by column chromatography on silica gel (eluent, petroleum ether: dichloromethane = 9:1, v/v) and recrystallized from n-hexane to yield **Br-STr** as pure white needle-like crystals (2.33 g, 67% yield).

^{1}H NMR (400 MHz, $CDCl_3$), Fig. S2. Δ 7.42 (d, *J* = 7.7 Hz, 6H), 7.31–7.26 (m, 6H), 7.20 (t, *J* = 7.2 Hz, 3H), 3.40 (t, *J* = 6.8 Hz, 2H), 2.13 (t, *J* = 7.2 Hz, 2H), 1.87–1.80 (m, 2H), 1.43–1.35 (m, 4H), 1.30–1.12 (m, 10H).

Step 2. Synthesis of (*E*)-1-(4-((10-((trityl)thio)decyl)oxy)phenyl)-2-phenyldiazene (azo-STr)

In a 100 mL round-bottom flask, 4-hydroxyazobenzene (0.198 g, 1 mmol), **Br-STr** (0.495 g, 1 mmol), and potassium carbonate (0.414 g, 3 mmol) were combined in 50 mL of acetonitrile. The reaction system was refluxed at 80 °C overnight under a nitrogen atmosphere. Upon completion, the reaction was cooled to room temperature. The solvent was removed by rotary evaporation, and the residue was dissolved in dichloromethane. The crude product was purified by column chromatography on silica

gel (eluent, petroleum ether: dichloromethane = 20:1, v/v) to obtain **azo-STr** (0.50 g, 79% yield).

^{1}H NMR (400 MHz, $CDCl_3$), Fig. S3. Δ 7.93 (d, *J* = 7.7 Hz, 2H), 7.88 (d, *J* = 7.7 Hz, 2H), 7.52 (t, *J* = 7.6 Hz, 2H), 7.48–7.40 (m, 8H), 7.30 (t, *J* = 7.8 Hz, 8H), 7.02 (d, *J* = 7.7 Hz, 2H), 4.06 (t, *J* = 7.0 Hz, 2H), 2.16 (q, *J* = 7.0 Hz, 2H), 1.84 (p, *J* = 7.0 Hz, 2H), 1.60–1.12 (m, 14H).

Step 3. Synthesis of (*E*)-1-(4-((10-mercaptodecyl)oxy)phenyl)-2-phenyldiazene (AZO ligand)

In a 10 mL round-bottom flask, 0.50 g of **azo-STr**, 1 mL of triethylsilane, and 100 μL of trifluoroacetic acid were added. The solution turned red, and the reaction was allowed to proceed for 30 minutes before being quenched with water. The crude product was purified by column chromatography (silica gel, petroleum ether/CH_2Cl_2 = 10/1, v/v) to afford **AZO ligand** as a pale-yellow solid (0.24 g, 80% yield).

^{1}H NMR (400 MHz, $CDCl_3$), Fig. S4. δ 7.93 (d, *J* = 7.6 Hz, 2H), 7.89 (d, *J* = 7.7 Hz, 2H), 7.52 (t, *J* = 7.6 Hz, 2H), 7.46 (t, *J* = 7.6 Hz, 1H), 7.03 (d, *J* = 7.7 Hz, 2H), 4.07 (t, *J* = 6.7 Hz, 2H), 2.16 (q, *J* = 7.2 Hz, 2H), 1.84 (p, *J* = 6.8 Hz, 2H), 1.60–1.12 (m, 15H).

Ligand exchange process.

The ligand exchange procedure was adapted from Ref.[3] with minor modifications, and all operations were performed under ambient atmosphere. Typically, 2.5 mg of QDs were dispersed in chloroform (5 mg mL^{-1}), followed by the slow addition of 500 μL of

AZO ligand solution in chloroform (20 mg mL^{-1}) under vigorous stirring. The mixture was stirred overnight to ensure complete ligand exchange. The ligand exchange duration can be slightly adjusted depending on the specific type of QDs. For instance, high-quality patterning can be achieved for red and green Cd-based QDs after only 1 hour of ligand exchange. In contrast, blue Cd-based QDs and InP-based red QDs require overnight stirring for binding sufficient number of AZO ligands and optimal patterning results. Also, extending the exchange duration does not significantly impact the patterning quality (Fig. S7). For most QD samples, overnight stirring is considered a suitable and versatile condition.

After the exchange, the QDs were purified by precipitation–redispersion cycles using toluene as the solvent and ethanol as the nonsolvent. Specifically, an equal volume of ethanol was added to the QD dispersion in toluene, followed by centrifugation to precipitate the QDs. The supernatant containing excess free ligands was discarded, and the QDs were redispersed in toluene. This washing procedure was repeated twice until the supernatant became completely colorless. The final purified QDs were stored as a stable dispersion in toluene.

Quantification of ligand density.

1. Ligand density before ligand exchange.

TEM analysis indicated that the average diameter of the CdSe/ZnS QDs was 13 nm. The QDs were assumed to be in a spherical geometry and a density of $\rho_{\mathrm{QD}} =$

5.0 g cm^{-3}. The molecular weight of oleic acid (OA) is $M_{\mathrm{OA}} = 282.5$ g mol^{-1}

The surface area and volume of a single QD are given by $A_{QD} = 4\pi r^2 = 531$ nm^2, $V_{QD} = \frac{4}{3}\pi r^3$, leading to a QD mass of

$$m_{\mathrm{QD}} = \rho_{\mathrm{QD}} V_{\mathrm{QD}} = 5.75 \times 10^{-18}\ \mathrm{g}$$

Thermogravimetric analysis (TGA) revealed a ligand-to-QD mass ratio of $m_{\mathrm{OA}}/m_{\mathrm{QD}} = 0.126$. Thus, the mass of OA per QD is

$$m_{\mathrm{OA}} = 0.1259\, m_{\mathrm{QD}} = 7.23 \times 10^{-19}\ \mathrm{g}$$

The corresponding number (N_{OA}) of OA molecules is

$$n_{\mathrm{OA}} = \frac{m_{\mathrm{OA}}}{M_{\mathrm{OA}}} \approx 2.56 \times 10^{-21}\ \mathrm{mol}$$

$$N_{\mathrm{OA}} = n_{\mathrm{OA}} N_{\mathrm{A}} \approx 1.54 \times 10^{3}$$

where N_{A} is Avogadro's number.

The surface ligand density is

$$\sigma = \frac{N_{\mathrm{OA}}}{A_{QD}} \approx 2.9\ \mathrm{nm}^{-2}$$

2. Ligand density after ligand exchange (AZO/OA dual ligands)

Similarly, for QDs after ligand exchange, the average diameter was still 13 nm. The QDs were again assumed to be a spherical geometry and a density of $\rho_{\mathrm{QD}} = 5.0$ g cm^{-3}. The molecular weights of the two ligands are $M_{\mathrm{AZO}} = 370.6$ g mol^{-1} and $M_{\mathrm{OA}} =$

282.5 g mol^{-1}. ^{1}H NMR analysis indicated a molar ratio of $n_{\mathrm{AZO}}:n_{\mathrm{OA}} = 0.95$. The QD surface area and mass are the same as above:

$$A_{QD} = 4\pi r^2 = 531\ \mathrm{nm}^2$$

$$m_{\mathrm{QD}} = \rho_{\mathrm{QD}} V_{\mathrm{QD}} = 5.75 \times 10^{-18}\ \mathrm{g}$$

TGA gave a total ligand-to-QD mass ratio of $m_{\mathrm{AZO+OA}}/m_{\mathrm{QD}} = 0.169$, corresponding to a total ligand mass per QD of

$$m_{\mathrm{AZO+OA}} = 0.169\, m_{\mathrm{QD}} \approx 9.71 \times 10^{-19}\ \mathrm{g}$$

From the molar ratio, $\frac{m_{\mathrm{OA}}}{M_{\mathrm{OA}}}:\frac{m_{\mathrm{AZO}}}{M_{\mathrm{AZO}}} = 0.95$, the ligand distribution was obtained as

$$n_{\mathrm{AZO}} = 1.46 \times 10^{-21}\ \mathrm{mol}$$

$$n_{\mathrm{OA}} = 1.53 \times 10^{-21}\ \mathrm{mol}$$

The corresponding number of molecules per QD is

$$N_{\mathrm{AZO}} = n_{\mathrm{AZO}} N_{\mathrm{A}} \approx 876$$

$$N_{\mathrm{OA}} = n_{\mathrm{OA}} N_{\mathrm{A}} \approx 923$$

Finally, the surface ligand densities are

$$\sigma_{\mathrm{AZO}} = \frac{N_{\mathrm{AZO}}}{A_{\mathrm{QD}}} \approx 1.65\ \mathrm{nm}^{-2}$$

$$\sigma_{\mathrm{OA}} = \frac{N_{\mathrm{OA}}}{A_{\mathrm{QD}} A_{\mathrm{QD}}} \approx 1.74\ \mathrm{nm}^{-2}$$

The calculated surface densities before and after ligand exchange are both close

to 3 nm^{-2}. This indicates that ligand exchange replaces OA with AZO ligands in nearly a one-to-one manner, without significantly altering the overall ligand coverage of the QD surface.

Direct photopatterning and erasing procedures

All patterning and erasing processes were conducted in ambient air. Silicon wafers and quartz substrates were first wiped with a dust-free cloth, then ultrasonically cleaned sequentially in toluene, acetone, methanol, and isopropanol for 15 minutes each. Finally, the substrates were dried under nitrogen flow before use.

For the patterning process, QDs with AZO/OA dual ligands (typically 25 mg mL^{-1}) were washed twice (toluene/ethanol as the solvent/nonsolvent pair), and then spin-coated onto a substrate at 1500 rpm for 30 s. Subsequently, the QD film was placed in a mask aligner (XT-01-UV mask aligner, Zhongxinrecheng Science and Technology Co. Ltd.) and brought into close contact with a pre-designed photomask. The film was then exposed to 365 nm UV light with a typical dose of 300 mJ cm^{-2}. After exposure, the uncrosslinked regions were removed by a dynamic washing process: while the substrate was spinning at 1500 rpm, 50 μL of toluene was dispensed onto it. For multicolor patterning, the process was repeated to deposit a subsequent layer after the completion of the single-step patterning. The optimal exposure dose was 300 mJ cm^{-2} for red and green Cd-based and InP QDs, and 500 mJ cm^{-2} for blue Cd-based QDs. All QD patterns were developed under the same conditions.

The erasing process was an additional step performed after the initial patterning. Specifically, after the first UV exposure (365 nm, 300 mJ cm^{-2}) and dynamic washing, the patterned QD film was returned to the mask aligner and covered with a second, different pre-designed photomask. The film was then exposed to 405 nm or 450 nm light with a typical dose of 500 mJ cm^{-2}. Following this second exposure, the newly exposed regions were removed using the same dynamic washing method (dispensing 50 μL of toluene onto the substrate spinning at 1500 rpm).

Characterization techniques

UV–visible absorption spectra of AZO ligands and QDs were recorded using an Agilent Cary 5000 UV–Vis–NIR spectrophotometer. ^{1}H NMR spectra were measured on a JEOL JNM-ECZ400S spectrometer (400 MHz). Transmission electron microscopy (TEM) images of QDs were obtained on a Hitachi HT-7700 microscope operated at 100 kV. Fluorescence microscopy images of patterned QDs were acquired using a Nikon Ni-U fluorescence microscope, and the film thicknesses were measured with a Bruker Dektak-XT profilometer. Scanning electron microscopy (SEM) images of pristine and patterned QD films were collected on a Hitachi SU-8010 microscope at 10 kV, and atomic force microscopy (AFM) images were obtained using a Bruker Dimension ICON or an Oxford Cypher S system. Thermogravimetric analysis (TGA) was performed on a Mettler Toledo TGA/DSC1/1600LFT instrument at a heating rate of 10 ^{o}C min^{-1} under nitrogen flow. Photoluminescence (PL) spectra of QDs were measured

using a Horiba FluoroMax Plus spectrometer, and absolute PLQYs at various patterning and erasing stages were determined using a 3.2-inch integrating sphere (excitation at 390 nm for both red- and green-emitting QDs). Time-resolved PL decay curves were collected using the same FluoroMax Plus system equipped with a TCSPC module, with excitation wavelengths of 393 nm for red- and green-emitting QD films. QD films for PL lifetime measurements were prepared by spin-coating 30 mg mL^{-1} QD solutions on quartz substrates at 2000 rpm. After subtracting background signals, PL decay curves at different patterning stages were recorded under identical conditions and fitted using the instrument's built-in software, with fitting equations summarized in Table S1.

Device fabrication and test

Bottom-emitting QLEDs with the structure glass/ITO/PEDOT:PSS/TFB/QDs/ZnMgO/Ag were fabricated inside a N_2-filled glovebox, using ITO and Ag as the anode and cathode, respectively. Prior to device fabrication, patterned ITO substrates (≈50 Ω sq^{-1}) were sequentially cleaned by ultrasonic treatment in tergitol/DI water solution, DI water, and isopropanol, followed by ultraviolet–ozone treatment for 15 min. A ≈40 nm PEDOT:PSS layer was spin-coated onto the cleaned ITO substrates and annealed at 150 ºC for 30 min. Subsequently, a ≈30 nm TFB layer was deposited from a TFB/chlorobenzene solution and annealed at 200 ºC for 30 min. To ensure solvent compatibility with the QD/toluene ink, the TFB film was further subjected to a crosslinking process optimized for toluene-based solvents, enabling robust film integrity during subsequent QD deposition. A ≈25 nm QD emission layer and a ≈30 nm ZnMgO electron-transport layer were sequentially deposited from QD/toluene and

ZnMgO/butanol solutions, and annealed at 100 ºC and 120 ºC for 10 min, respectively. Finally, a 100 nm Ag cathode was deposited by thermal evaporation under high vacuum. The active emitting area of each device was 0.04 cm^2. All devices were encapsulated inside the glovebox using a UV-curable epoxy and a cover glass. Pristine devices employed a QD layer formed by direct spin-coating of dual-ligand-capped QDs. In contrast, patterned devices were processed by spin-coating, 365-nm flood exposure (300 mJ cm^{-2}), and subsequent toluene development. The *J–V–L* and EQE characteristics and operational stability were measured using custom-built LabView-controlled characterization platforms. The setup included a QE-PRO fiber-optic spectrometer, Keithley 2400/6485 source meters, a probe station inside a light-tight chamber, and signal/data acquisition modules, enabling simultaneous collection of voltage, current density, luminance, and EL spectra. External quantum efficiency, power efficiency, and related parameters were calculated from the measured electrical and optical data. Device lifetime testing was performed using a stability measurement system equipped with a Keithley 2400 source meter, a CS-160 luminance meter for absolute calibration, a photodiode detector, and a temperature-controlled chamber. Devices were driven under constant voltage or constant current while their emission intensity was continuously monitored by the photodiode, and the recorded evolution of luminance was used to extract operational lifetime.

Supplementary discussion on the interparticle interactions

As a representative case, we focus on the red-emitting dual-ligand QDs. Based on ^1H

NMR quantification and TGA analysis (Fig. S10), a QD with a diameter of ≈13 nm carries approximately 876 AZO ligands together with 923 native ligands on the surface. The AZO ligands undergo reversible *trans–cis* photoisomerization, which results in a substantial change in their permanent dipole moment. This dipole change modifies the dipole – dipole interaction between neighboring ligands located on adjacent QDs, thereby altering the interparticle attraction.

To estimate this effect, we evaluate the dipole–dipole interaction energy ($\varepsilon_{\mathrm{DD}}$) between two *cis*-AZO ligands. According to Ref.[4], $\varepsilon_{\mathrm{DD}}$ is expressed as

$$\varepsilon_{\mathrm{DD}} = (-1/3k_{\mathrm{B}}T)(\mu^2/4\pi\varepsilon_0\varepsilon a^3)^2$$

where a is the separation distance between two dipoles (taken as 5 Å, corresponding to closest dipole-dipole spacing, according to Ref.[4]), $\mu = 2.7$ D is the dipole moment of *cis*-AZO ligand[4], $\varepsilon = 2.379$ is the dielectric constant of toluene, and ε_0 is the vacuum permittivity. Substituting the values gives $\varepsilon_{\mathrm{DD}} \approx -0.12k_{\mathrm{B}}T$.

Under typical photopatterning conditions (365 nm UV light, 300 mJ cm^{-2}), about 95% of the surface AZO ligands undergo *trans*-to-*cis* isomerization ($\chi_{\mathrm{cis}} = 0.95$), as confirmed by data from UV–Vis spectra (Fig. S11). From the analysis in **Quantification of ligand density** part, the ligand density after ligand exchange is $\sigma_{\mathrm{AZO}} = 1.49$ nm^2. The dipole–dipole induced interparticle interaction energy (U_{DD}) can be estimated as

$$U_{\mathrm{DD}} \approx \chi_{\mathrm{cis}} A_{\mathrm{eff}} \varepsilon_{\mathrm{DD}} \sigma_{\mathrm{AZO}}$$

where A_{eff} represents the effective interacting area between two spheres of radius R, given by $A_{\mathrm{eff}} = 2\pi Ra$.

Substituting these values gives $U_{\mathrm{DD}} \approx -3.5\, k_{\mathrm{B}}T$ under typical photopatterning conditions, which is larger than the thermal kinetic energy of the QD.

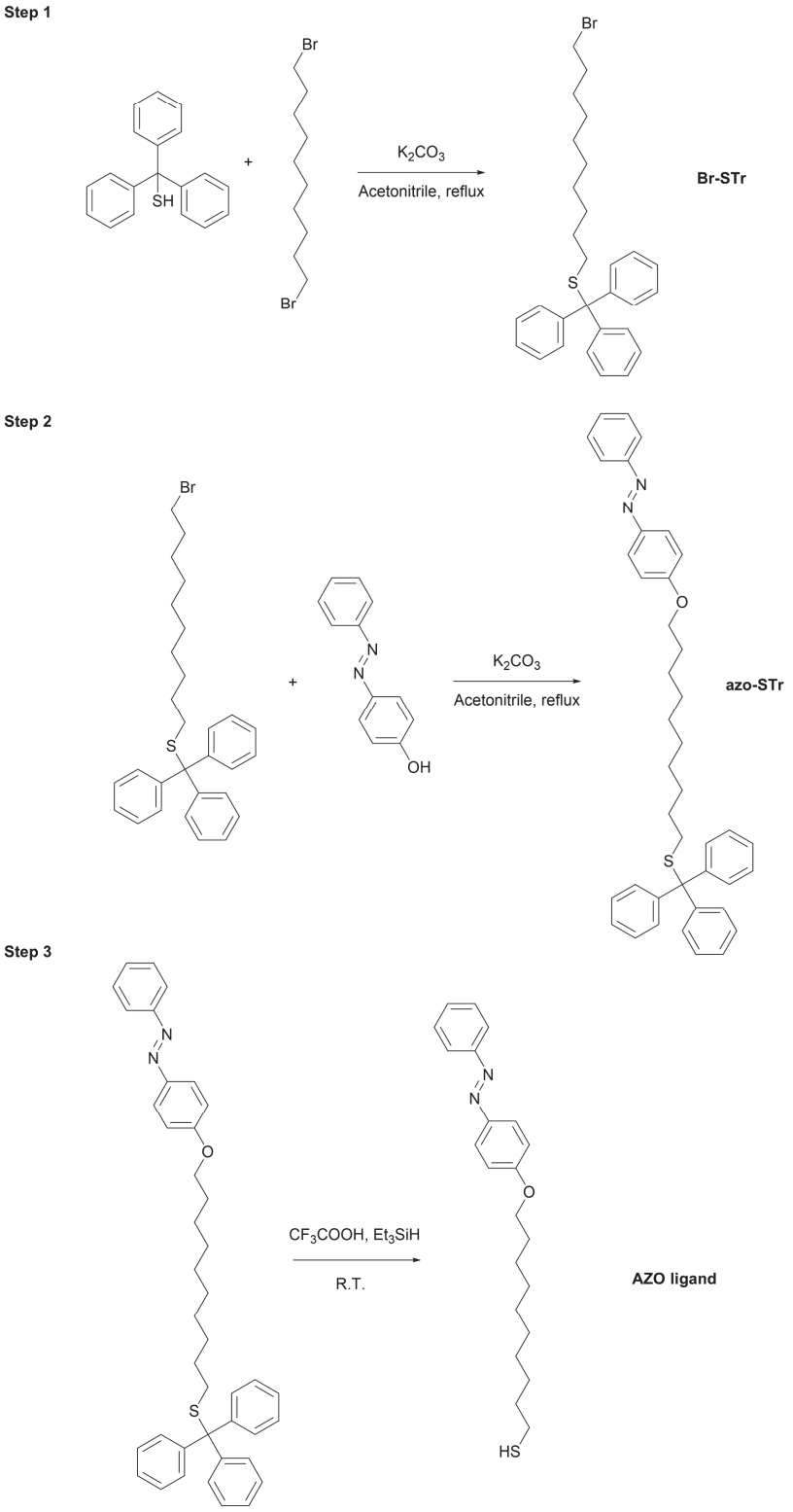

Fig. S1. The synthetic route of AZO ligand.

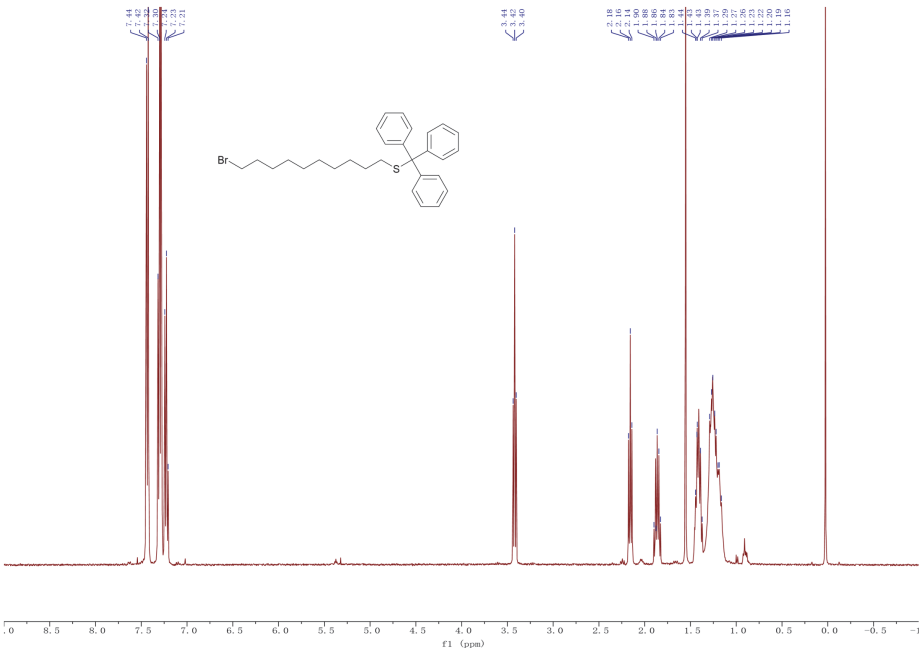

Fig. S2. The ^{1}H-NMR spectrum of Br-STr. The resonance at 7.26 ppm corresponds to residual protons in $CDCl_3$ and the resonance at 1.56 ppm corresponds to protons of H_2O.

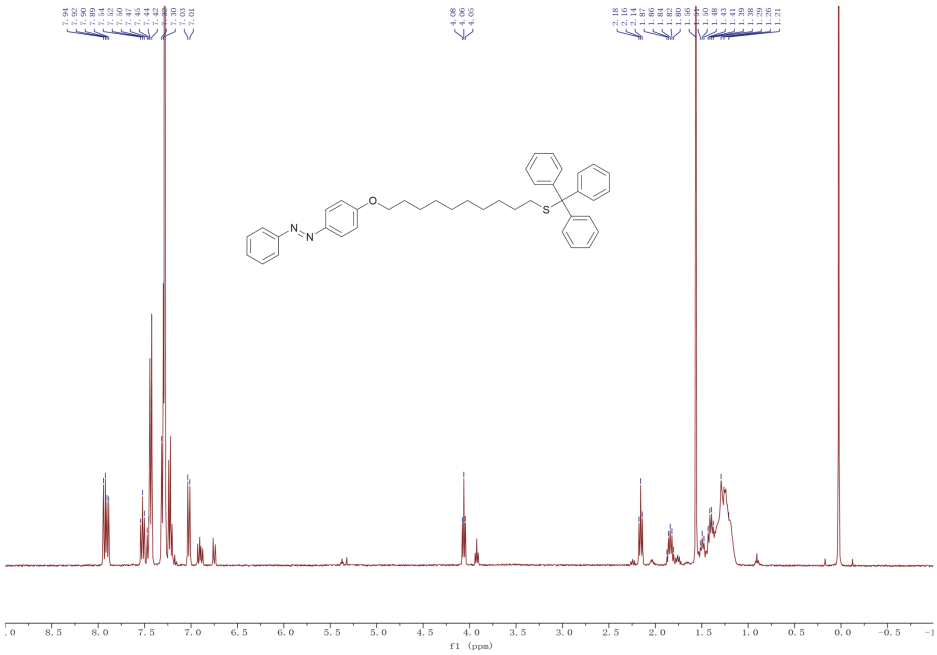

Fig. S3. The ^{1}H-NMR spectrum of azo-STr. The resonance at 7.26 ppm corresponds to residual protons in $CDCl_3$ and the resonance at 1.56 ppm corresponds to protons of H_2O.

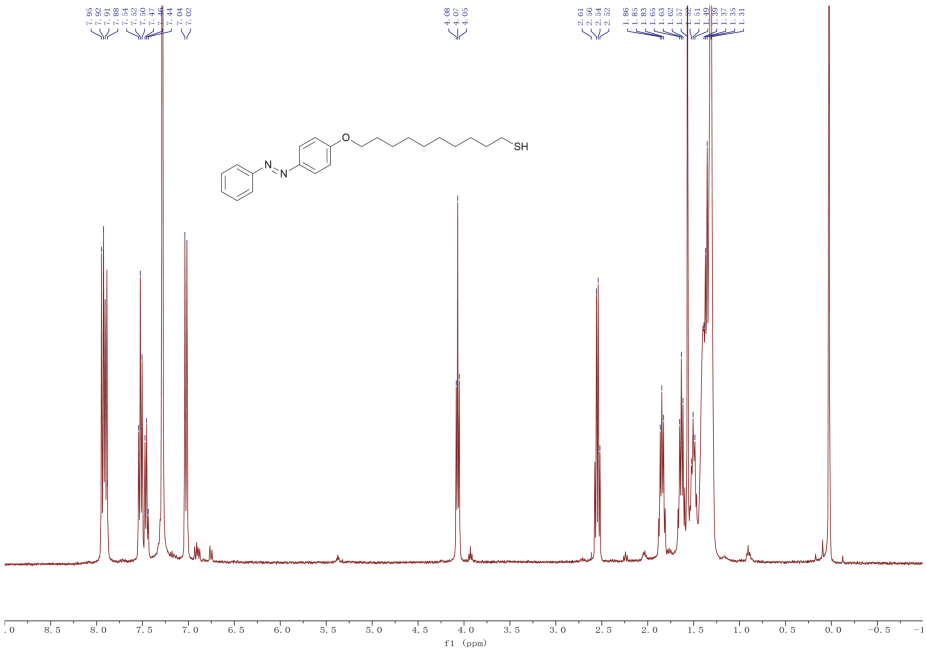

Fig. S4. The ^{1}H-NMR spectrum of AZO ligand. The resonance at 7.26 ppm corresponds to residual protons in $CDCl_3$ and the resonance at 1.56 ppm corresponds to protons of H_2O.

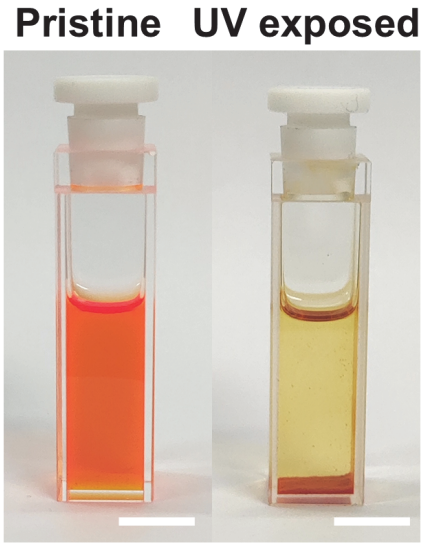

Fig. S5 Photographs of QD dispersions before and after 365 nm UV irradiation. Scale bar, 10 mm.

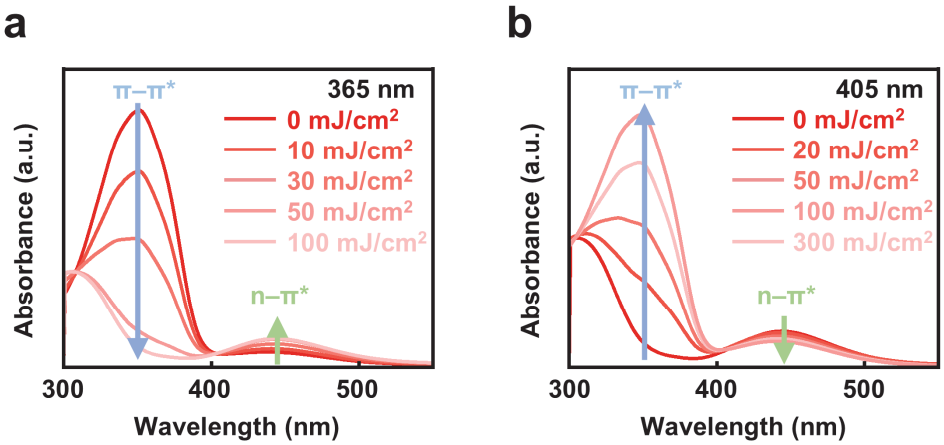

Fig. S6. UV–visible absorption spectra of AZO ligands in toluene under irradiation of different wavelengths. (a) 365 nm UV irradiation and (b) 405 nm visible light irradiation. Under 365-nm illumination (0–100 mJ cm^{-2}), the π–π* transition at ~350 nm progressively decreases while the n–π* transition at ~450 nm increases, indicating dose-dependent *trans*–to–*cis* photoisomerization. In contrast, 405-nm irradiation (0–300 mJ cm^{-2}) induces the reverse *cis*–to–*trans* back-isomerization, evidenced by the recovery of the π–π* band and the reduction of the n–π* transition.

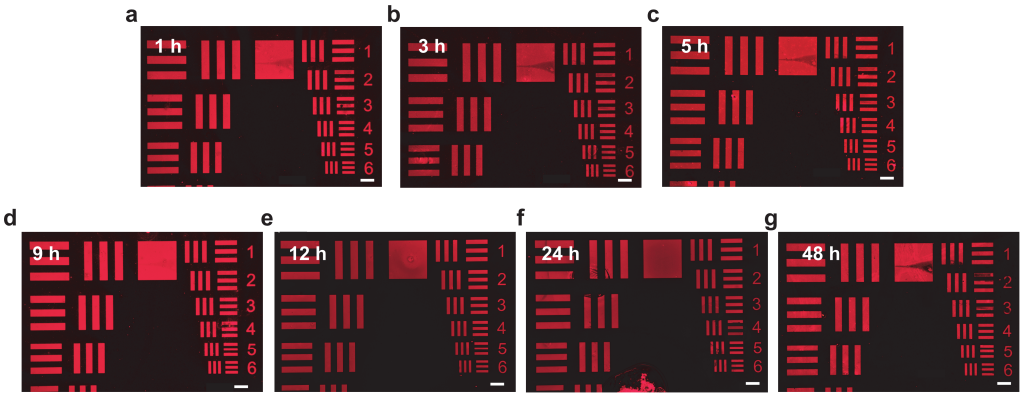

Fig. S7. Influence of ligand exchange duration on the photopatterning quality of QDs. Fluorescence micrographs of patterned red-emitting Cd-based QDs obtained after various ligand exchange times: 1, 3, 5, 9, 12, 24, and 48 h. All samples exhibit high-fidelity patterns with sharp resolution, demonstrating a robust processing window for the ligand-exchange-mediated photopatterning protocol. Scale bars, 200 μm

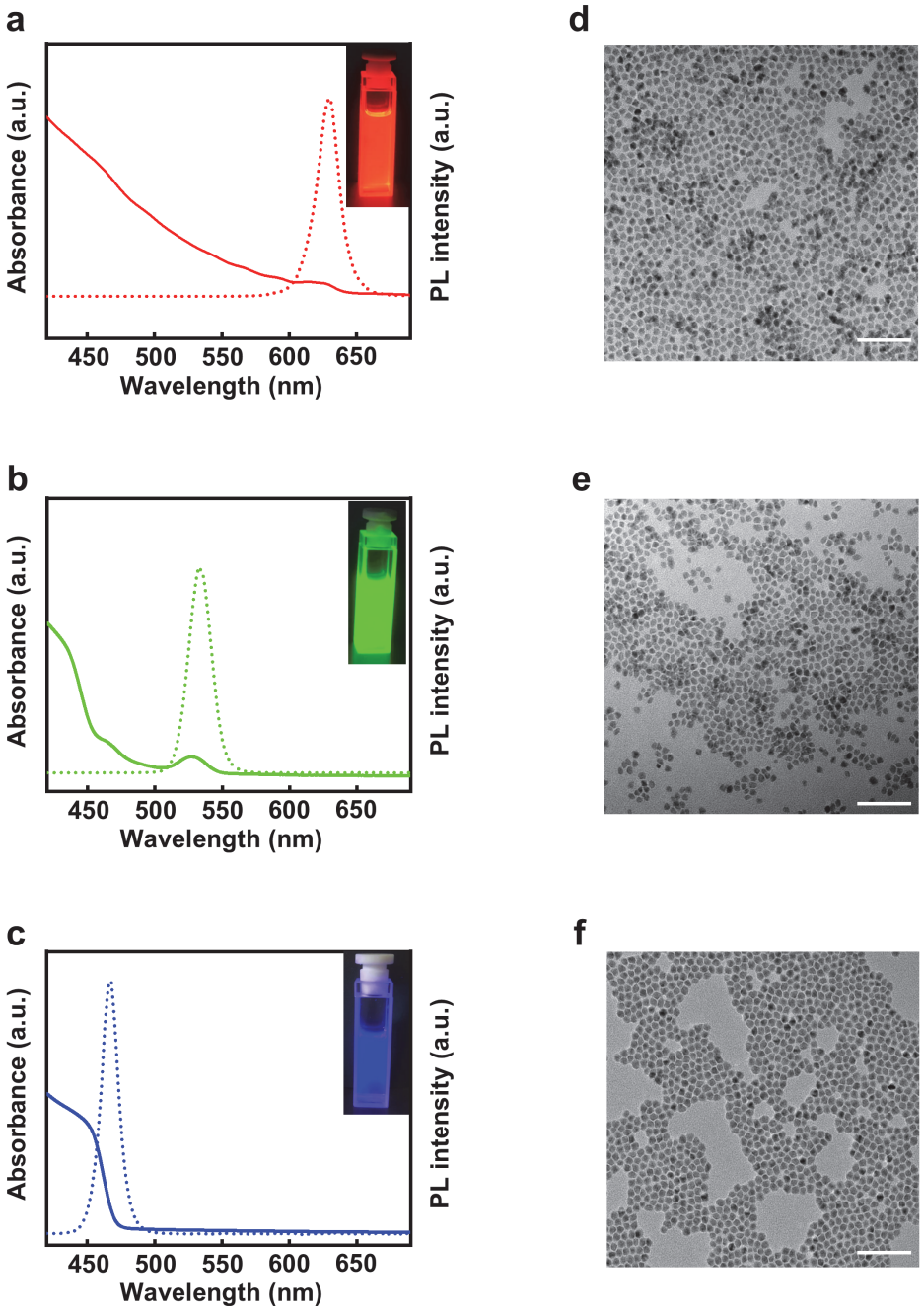

Fig. S8. Optical properties and morphology of QDs. (a–c) UV–visible absorption, PL spectra and photos under UV light of R (CdZnSe/CdZnS/ZnS), G (CdZnSe/ZnSe/ZnS), and B (CdZnSe/ZnS) QDs. (d–f) TEM images of corresponding QDs. Scale bars, 100 nm.

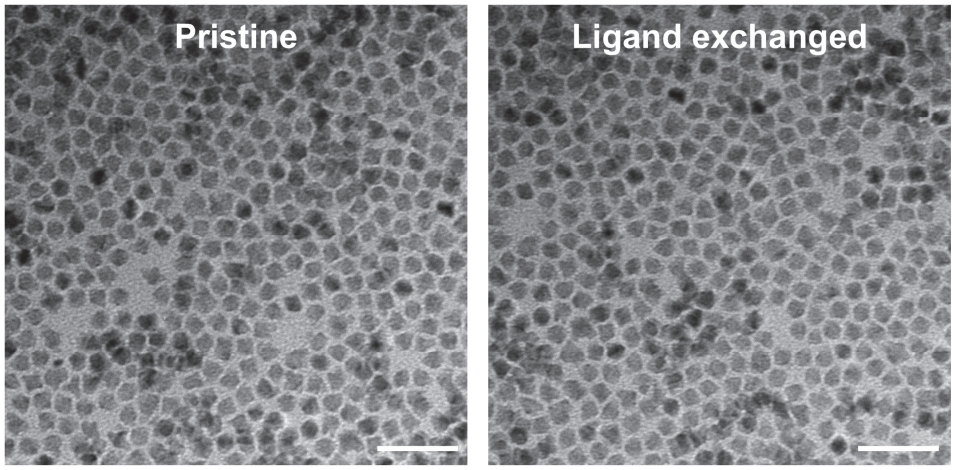

Fig. S9. TEM images of the QDs before and after ligand exchange. QDs retain their morphology and size distribution after ligand exchange, indicating that the exchange process does not induce noticeable structural changes. Scale bars, 50 nm.

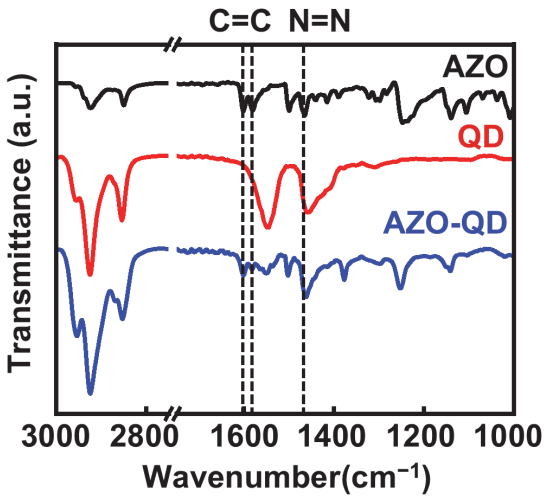

Fig. S10. FTIR spectra of pure AZO ligands, pristine QDs and QDs with dual ligands (AZO-QD), confirming successful ligand exchange.

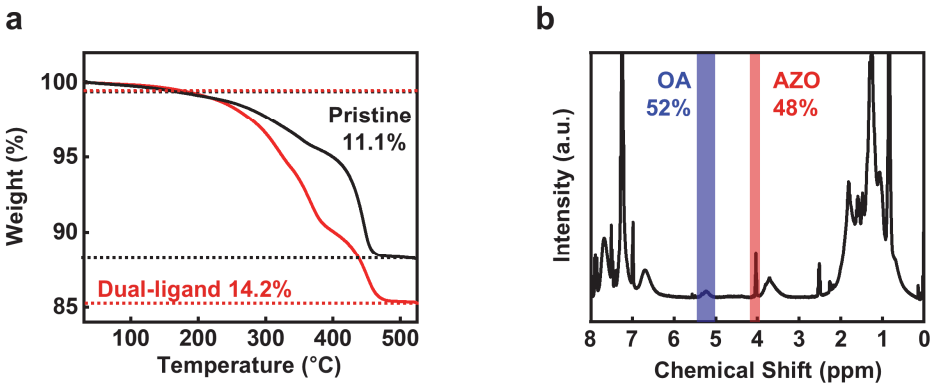

Fig. S11. Quantitative analysis of ligand exchange. (a) TGA of pristine (black line) and dual-ligand capped (red line) red-emitting QDs. **(b)** ^{1}H-NMR spectrum of dual-ligand capped red-emitting QDs. The peaks in the red region correspond to the protons at the α-position to the ether oxygen on the AZO ligand, while the peaks in the blue region are attributed to the olefinic protons of the oleic acid ligand. The ratio of their integral areas reflects the proportion of the two ligands on the QD surface.

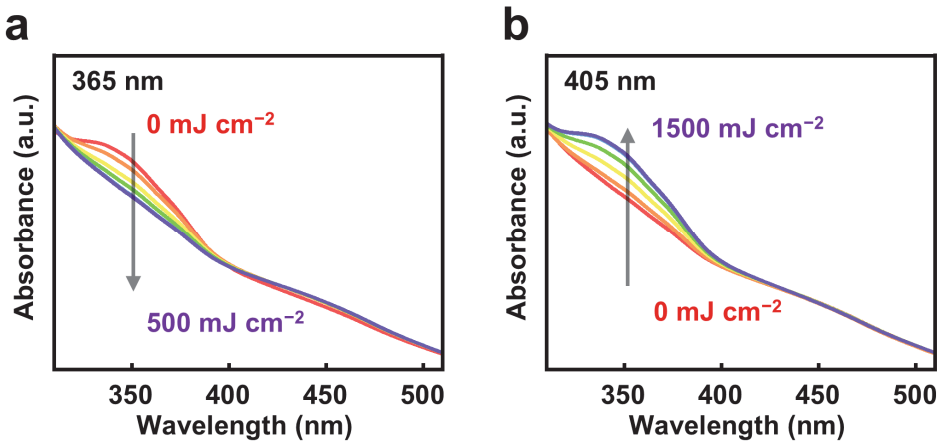

Fig. S12. UV–visible absorption spectra of AZO-QDs in toluene under irradiation of different wavelengths. (a) 365 nm exposure, demonstrating progressive *trans-to-cis* conversion. The red, orange, yellow, green, blue, and purple curves correspond to exposure doses of 0, 5, 20, 100, 300, and 500 mJ cm^{-2}, respectively. (b) 405 nm exposure, confirming reversible photoisomerization. The red, orange, yellow, green, blue, and purple curves correspond to exposure doses of 0, 10, 100, 200, 500, and 1500 mJ cm^{-2}, respectively.

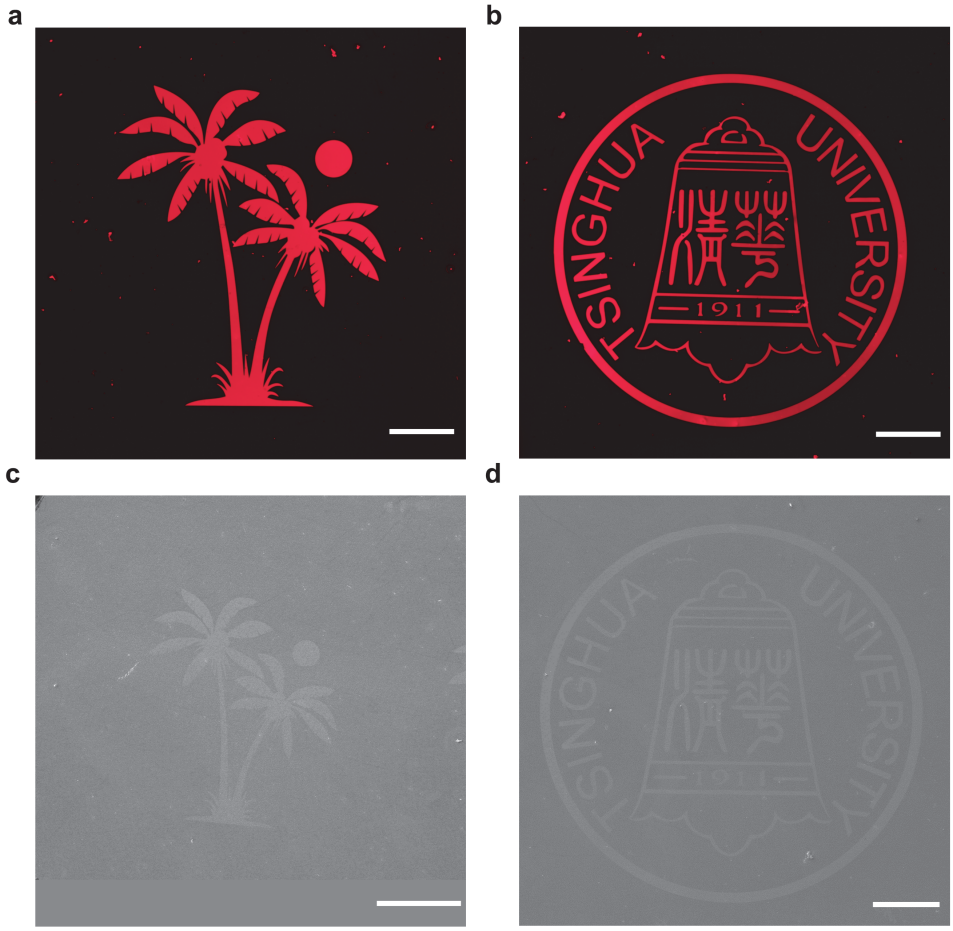

Fig. S13. Additional images of photopatterned QD films. (a,b) Fluorescence microscopy images of representative QD patterns produced using the photopatterning process, demonstrating high fidelity and uniform emission across complex motifs. (c,d) Corresponding SEM images of the same patterns. Scale bars, 200 μm.

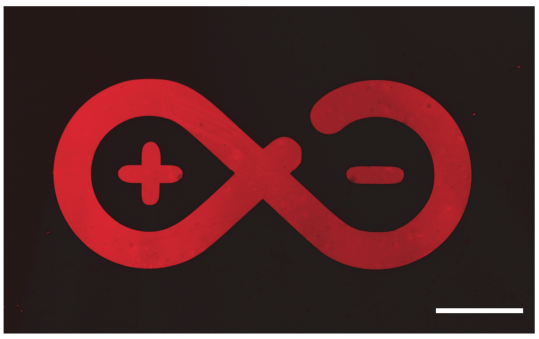

Fig. S14. Fluorescent images of patterns made by red-emitting InP/ZnSe/ZnS QDs. Scale bar, 100 μm.

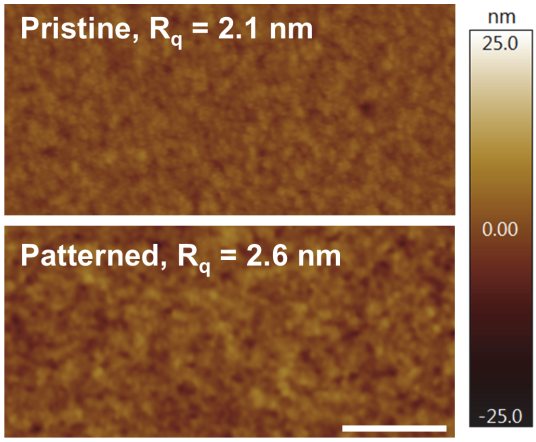

Fig. S15. AFM images of pristine and patterned QD films. Scale bar, 1 μm.

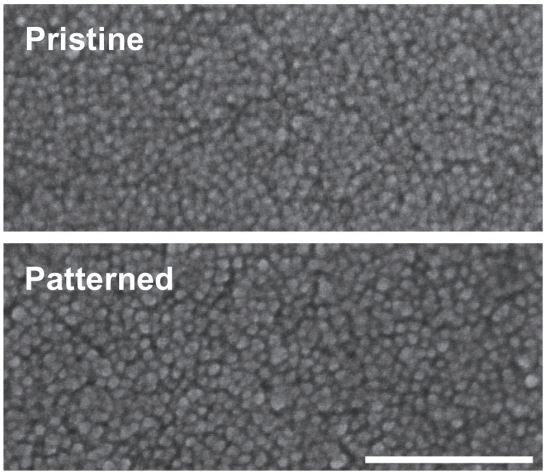

Fig. S16. SEM images of pristine and patterned films. Scale bar, 200 nm.

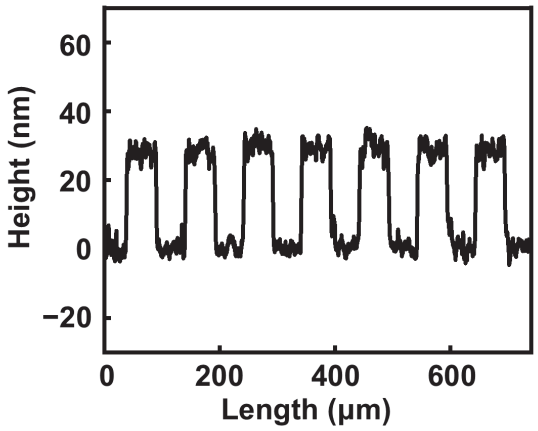

Fig. S17. Height profile of the patterned lines.

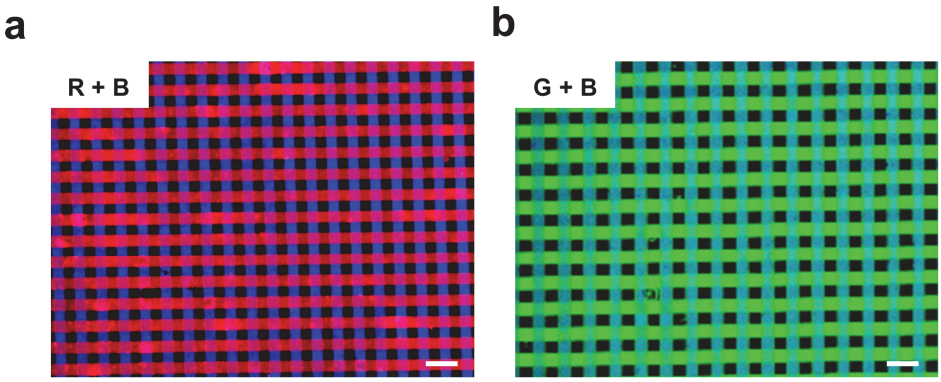

Fig. S18. Additional fluorescent images of multilayered QD patterns formed by sequential photopatterning. (a) Cross patterns of red- and blue-emitting QDs (R + B), and (b) Cross patterns of green- and blue-emitting QDs (G + B). Scale bars, 200 μm.

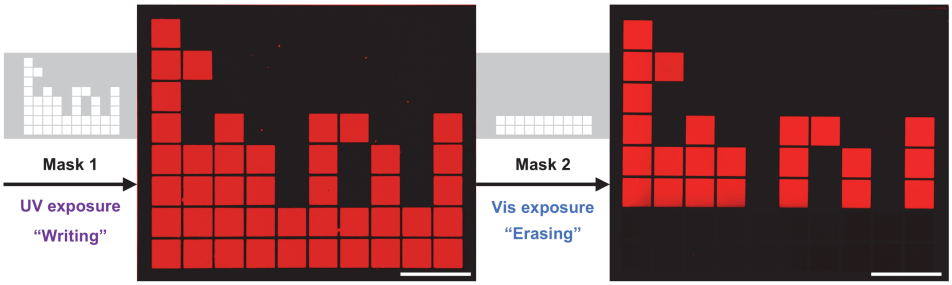

Fig. S19. The two-step "write–erase" procedure applied to form a Tetris-like pattern. UV writing creates the initial block arrangement, and visible-light erasing selectively removes lower rows to generate a new configuration. Scale bars, 100 μm.

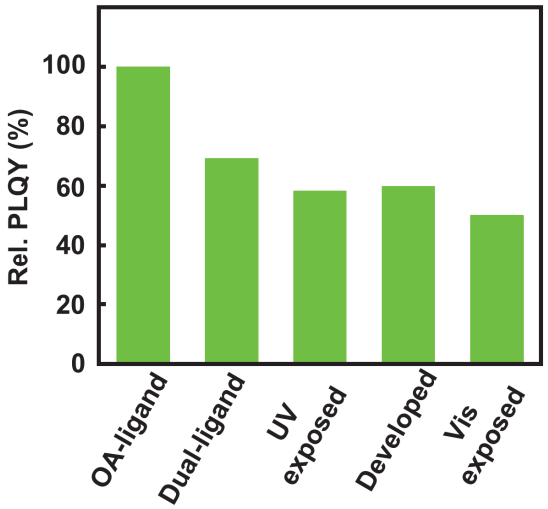

Fig. S20 Relative PLQYs of green-emitting QDs at different processing stages. These include pristine OA-ligand QDs, dual-ligand QDs, UV-exposed (365 nm), developed (toluene washing), and visible-light-exposed films (erasing condition).

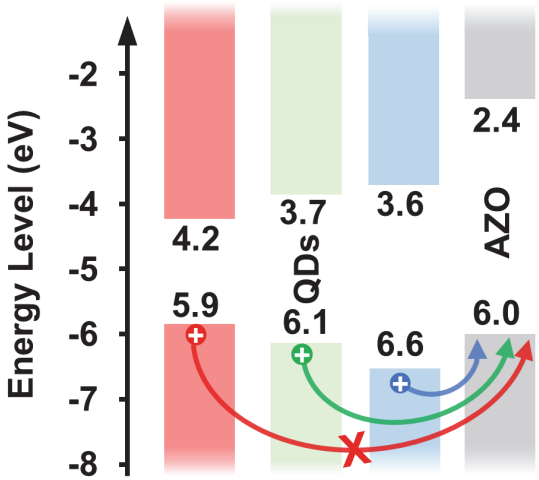

Fig. S21. Schematic energy level alignments of QDs of different colors and AZO ligands. The relatively shallow valence-band levels of blue and green QDs may facilitate hole transfer to the AZO ligand, leading to partial quenching of their photoluminescence. In contrast, the deeper valence band of red QDs suppresses this hole-transfer pathway, resulting in minimal PL loss. The edges of conduction band (CB) and valence band (VB) for QDs are from ref[5]. The HOMO/LUMO levels of the AZO ligand were obtained from Gaussian calculations.

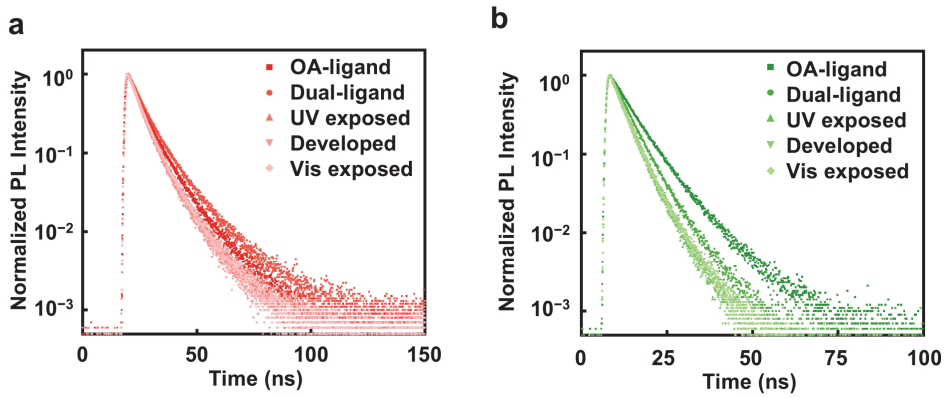

Fig. S22. Time-resolved PL decay curves of (a) red- and (b) green-emitting QDs at different processing stages. These include pristine OA-ligand QDs, dual-ligand QDs, UV-exposed (365 nm), developed (toluene washing), and visible-light-exposed films (erasing condition).

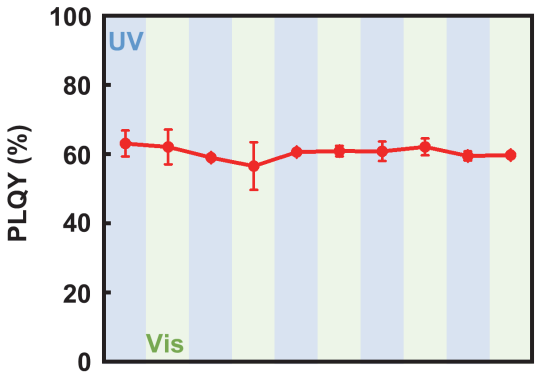

Fig. S23. PLQY stability of dual-ligand QDs over five cycles of alternating UV (*trans*–to–*cis*) and visible-light (*cis*–to–*trans*) switching.

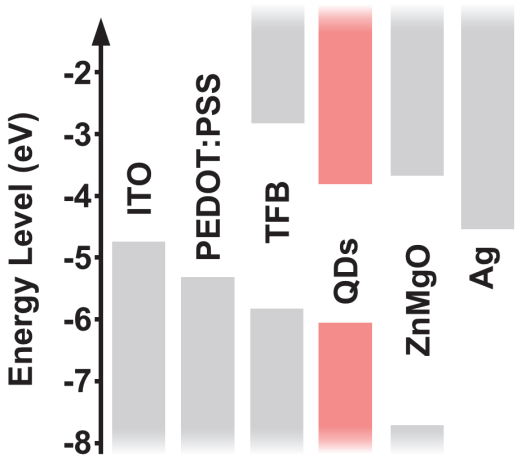

Fig. S24. Energy-level diagram of the QLED functional layers.

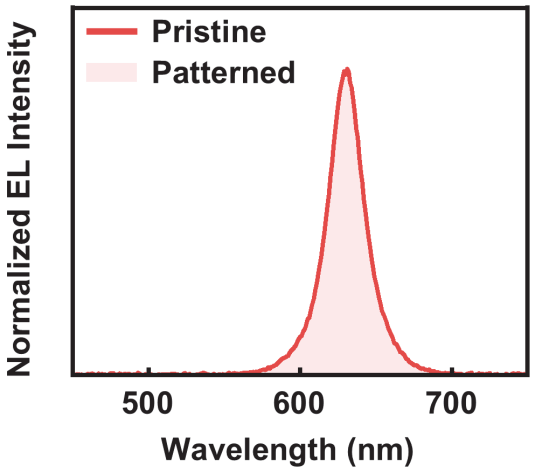

Fig. S25. Normalized EL spectra of pristine and patterned QLEDs.

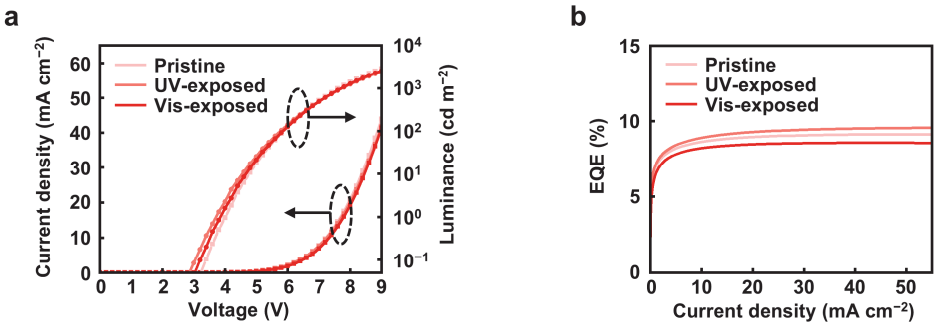

Fig. S26. Influence of AZO ligand trans–cis–trans photoisomerization on the EL performance of QLEDs. (a) *J–V–L* characteristics and (b) EQE versus current density for QLEDs in the pristine (*trans*-AZO), UV-exposed (*cis*-AZO), and Vis-exposed (*trans*-AZO) states.

Table S1. Fitting parameters for time-resolved PL of QD films with different treatments. These include pristine, ligand exchanged, UV exposed, developed and Vis exposed. τ_{avg} represents the averaged lifetime of samples.
Rel. B_1 and Rel. B_2 represent the relative percentage or amplitude of the two decays in the bi-exponential fitting of the time-resolved PL. The average PL lifetime (τ_{avg}) of were measured with TCSPC toolkit on a Horiba FluoroMax Plus spectrometer and the fitting follows $y = A + B_1 e^{\left(-\frac{x}{\tau_1}\right)} + B_2 e^{\left(-\frac{x}{\tau_2}\right)}$.

Sample		τ_1 (ns)	Rel. B_1 (%)	τ_2 (ns)	Rel. B_2 (%)	τ_{avg} (ns)
RQD	OA-ligand	4.83	57.13%	12.35	42.87%	**6.54**
	Dual-ligand	5.42	57.19%	14.10	42.81%	**7.36**
	UV exposed	4.62	64.82%	11.48	35.18%	**5.85**
	Developed	4.15	59.26%	10.35	40.74%	**5.50**
	Vis exposed	4.27	56.91%	10.62	43.09%	**5.75**
GQD	OA-ligand	3.01	28.10%	7.90	71.90%	**5.43**
	Dual-ligand	3.43	11.46%	6.63	88.54%	**3.87**
	UV exposed	1.37	20.89%	4.49	79.11%	**3.04**
	Developed	4.05	82.35%	7.97	17.65%	**4.44**
	Vis exposed	3.13	46.56%	6.95	53.44%	**4.43**

Reference

1 Z. Yang, P.-A. Cazade, J.-L. Lin, Z. Cao, N. Chen, D. Zhang, L. Duan, C. A. Nijhuis, D. Thompson and Y. Li, *Nat. Commun.*, 2023, **14**, 5639.

2 J. Lin, Z. Cao, X. Bai, N. Chen, C. Li, X. Xiao, L. Wang and Y. Li, *Adv. Mater. Interfaces*, 2022, **9**, 2201238.

3 D. Hahm, J. Lim, H. Kim, J.-W. Shin, S. Hwang, S. Rhee, J. H. Chang, J. Yang, C. H. Lim, H. Jo, B. Choi, N. S. Cho, Y.-S. Park, D. C. Lee, E. Hwang, S. Chung, C. Kang, M. S. Kang and W. K. Bae, *Nat. Nanotechnol.*, 2022, **17**, 952–958.

4 R. Klajn, P. J. Wesson, K. J. M. Bishop and B. A. Grzybowski, *Angew. Chem. Int. Ed.*, 2009, **48**, 7035–7039.

5 E. Jang and H. Jang, *Chem. Rev.*, 2023, **123**, 4663–4692.